

Day-Ahead and Intra-Day Planning of Integrated BESS-PV Systems providing Frequency Regulation

Francesco Conte, *Member, IEEE*, Stefano Massucco, *Senior Member, IEEE*,
Giacomo-Piero Schiapparelli, *Student Member, IEEE*, and Federico Silvestro, *Senior Member, IEEE*

Abstract—The paper proposes an optimal management strategy for a system composed by a battery and a photovoltaic power plant. This integrated system is called to deliver the photovoltaic power and to simultaneously provide droop-based primary frequency regulation to the main grid. The battery state-of-energy is controlled by power offset signals, which are determined using photovoltaic energy generation forecasts and predictions of the energy required to operate frequency regulation. A two level control architecture is developed. A day-ahead planning algorithm schedules the energy profile which is traded at the day-ahead market and defines the primary control reserve that the integrated system is able to provide in the considered day. During the day operations, a second level algorithm corrects the dispatched plan using updated information, in order to guarantee a continuous and reliable service. Both control algorithms take into account the uncertainties of the photovoltaic generation and of the frequency dynamics using stochastic optimization.

Index Terms—Battery energy storage systems, primary frequency regulation, primary control reserve, predictive control, photovoltaic systems.

I. INTRODUCTION

THE instantaneous balance between generated and consumed active power is one of the basic principles of the AC power systems operation. Any variation from such a condition causes a frequency event, namely, the deviation of the system frequency from its nominal value. The progressive displacement of conventional generation in favour of production from Renewable Energy Sources (RES) will cause the reduction of the frequency control capability of power systems. Therefore, it is necessary to involve new resources in grid ancillary services in order to ensure robustness, resiliency and efficiency of future power systems [1]–[3].

The power equilibrium in real-time can be controlled only if the production system is able to change its generation level [4]. The coupling of RES with Battery Energy Storage Systems (BESSs) is therefore investigated in order to meet the grid flexibility requirements with the aleatory characteristics of such generation systems [5]–[7]. Assessments on the capital costs of batteries have shown that, with the market condition of last years, a multifunctional storage deployment is necessary to overcome the investment costs for energy storage systems [8].

F. Conte, S. Massucco, G.-P. Schiapparelli, F. Silvestro are with are with the Dipartimento di Ingegneria Navale, Elettrica, Elettronica e delle Telecomunicazioni, Università degli Studi di Genova, via all'Opera Pia, 11A , I-16145 Genova (GE), Italy, e-mail: fr.conte@unige.it, stefano.massucco@unige.it, giacomo-piero.schiapparelli@edu.unige.it, federico.silvestro@unige.it *Corresponding author*: Federico Silvestro

Corresponding author: Federico Silvestro

DOI: 10.1109/TSTE.2019.2941369

Many literature papers propose methods for allowing batteries to provide services such as energy management, peak shaving, and frequency and voltage regulation [9]–[23]. Several control strategies to perform Primary Frequency Regulation (PFR) are proposed in literature [24]–[26]. Moreover, specific markets around the world are now under development in order to integrate BESS into grid services, such as in the United States PJM interconnect and ISO New England [27], [28], in the Europe National Grid (GB) [29] and in the International Grid Control Cooperation (IGCC) which involves German, Belgian, Dutch, French, Swiss and Austrian Primary Control Reserve (PCR) markets [30].

In this work an integrated BESS-Photovoltaic system (PV) system is considered. A wide literature shows how to properly manage this Integrated System (IS) to perform multiple services such as contingency management, peak shaving, demand response, etc. [31]–[33]. However, in many cases droop-based PFR is not considered. Papers combining multiple services with PFR usually assume a non-traditional provision of PFR, such as the one defined by the PJM market [27]. In this specific case, the signal provided to the regulating units is divided in two contributions, a slow one (RegA) and a fast one (RegD). The one provided to BESS and RES is RegD, which is designed to be zero-mean, in order to keep the BESS State-Of-Charge (SOC) approximately at the same level, during a given time period [31], [32], [34]. Nevertheless, most markets do not adopt this control strategy, but use the row frequency as regulating signal, which is not guaranteed to be zero-mean within a given time period. In this case, more sophisticated techniques, such as the ones in [35] and [9] should be used.

In particular, in [35] and [9] PFR is coupled with the dispatch of the active power demand of a distribution feeder. Moreover, such as other works previously cited, these two works are focused on the usage of batteries in transmission and distribution level. Differently, the present paper is focused on the generation level: the IS is operated as a power plant which simultaneously participates to the energy market, delivering to the grid the available PV generation, and provide droop-based PFR. The main contribution of this work is therefore the integration of these two services with a common formulation. Moreover, the problem is defined in order to match the current grid codes and markets requirements (see Section II-B for details).

The IS architecture is depicted in Fig. 1. The objective is to define an energy dispatch plan using the storage flexibility, to maximize the economic gain and provide a continuous and reliable PFR service. A two level strategy [36] is adopted.

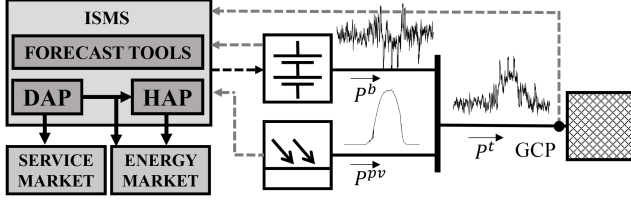


Fig. 1. Integrated system configuration scheme.

A suitably developed algorithm, called day-ahead planning (DAP), defines an energy dispatch plan and a droop coefficient for the up-coming day, both traded at the day-ahead market. DAP uses the forecasts of the PV generation and of the energy required to perform PFR. The latter information is provided by a method proposed in [35]. Then, during the day operation, an hour-ahead planning (HAP) algorithm corrects the DAP dispatch plan using updated short-term forecasts and the current battery State-Of-Energy (SOE), in order to assure the continuity of the PFR service. The dispatch plan corrections are traded at the intra-day energy market. Both DAP and HAP use chance-constrained optimization [37], in order to take into account the uncertainties of the PV generation and of the frequency signal dynamics.

It is worth remarking that the problem formulation is general, there are no hypotheses on the type of battery or its performance or the ratings of the resources. Moreover, there are neither hypothesis on the coupling between the BESS and the PV plants, that could be in principle in AC, DC or even the results of an aggregation of several BESSs and PVs.

The performances of the designed method are tested by simulations in MATLAB/Simulink, the test environment adopted has been validated by on field experiments as detailed in [35].

The rest of the paper is organized as follows. Section II describes the system configuration and provides the problem formulation. Section III and Section IV introduced the DAP and HAP algorithms, respectively. Simulation results are described in Section V. Finally, conclusions are reported in Section VI.

Notation. $\mathbf{E}(z)$ is the expectation of the random variable z ; $\mathbf{P}(A)$ is the probability of event A ; $x \sim \mathcal{N}(\bar{z}, \sigma^2)$ indicates that z is a Normally distributed random variable with mean \bar{z} and variance σ^2 ; $\text{erf}^{-1}(\cdot)$ is the inverse Gauss error function; $k = a : b$, denotes the sequence $k = a, a + 1, \dots, b$.

II. PROBLEM FORMULATION

The system configuration is presented in Fig. 1. The IS is composed by a BESS and a PV plant. The power P^t [kW] is exported at the Grid Coupling Point (GCP). As indicated, $P^t > 0$ means that the IS is exporting power. With the same convention, the BESS exports or import power P^b [kW] and the PV plant generates power P^{pv} [kW]. From the figure, it clearly follows that

$$P^t = P^b + P^{pv}. \quad (1)$$

The PV generation and the BESS power exchange are limited by the rated powers P_n^{pv} and P_n^b , respectively. The

IS rated power is indicated with $P_n^t = P_n^{pv} + P_n^b$. The BESS energy capacity is indicated with E_n [kWh].

The IS has the objective of exporting the PV generation and provide PFR. Therefore, P^t assumes the form

$$P^t = P^m - \alpha \Delta f, \quad (2)$$

where α [kW/Hz] is the *droop* coefficient, Δf [Hz] is the frequency deviation from the nominal value f_n and P^m [kW] is the IS *market* power, *i.e.* the power traded at the energy market. The duration of the energy market sessions, also called dispatch sampling time, will be indicated with τ [s].

It is assumed that the IS always operates as a generator, and therefore $P^m \geq 0$. A minimal droop coefficient α_{\min} is established. It is therefore required that

$$\alpha \geq \alpha_{\min}. \quad (3)$$

The value of α_{\min} , can be defined, for example, according to [38], where a generator with rated power P_n participating to PFR has to ensure a maximum statism b_p^{\max} [%], that corresponds to α_{\min} by the relation

$$b_p^{\max} = \frac{100}{\alpha_{\min}} \cdot \frac{P_n}{f_n}. \quad (4)$$

PFR is effectively operated only by BESS. Therefore, to obtain (2), it results that the battery power exchange is

$$P^b = P^m - P^{pv} - \alpha \Delta f. \quad (5)$$

The IS is controlled by a IS Management System (ISMS) that receives measurements and sends control set-points from/to the PV inverter and the Battery Management System (BMS), which controls the BESS. In particular, the ISMS receives the measurements of the current PV power generation P^{pv} and of the battery State-of-Energy, indicated with S [p.u.].

In this paper, the SOE dynamics is modelled by the following discrete-time system:

$$S_{k+1} = S_k - \frac{\tau}{3600 \cdot E_n} P_k^b. \quad (6)$$

Notice that (6) describes the dynamics of a BESS with unitary efficiency. It will be shown that such an assumption in the control algorithm design do not affect the overall results. The same approximation has been done and verified in [35], [39]

The ISMS has the mission of maximizing the economic gain coming from the energy delivery and the provision of the PFR service. It uses forecasts of the PV generation and of the energy required to provide PFR. Based on this information, each day, the ISMS trades the energy delivery profile and the day PFR droop coefficient α for the day-ahead. During the operation the battery SOE must be kept within the *security interval* $[S^{\min}, S^{\max}]$. The violation of the SOE security interval is called *failure*. When a failure occurs, the provision of PFR is suspended. The percentage time during which the SOE security interval is violated is defined *failure rate*, indicated with λ .

Using stochastic modelling, the *a priori* definition of maximal failure rate is, for all k ,

$$\lambda_{\max} = 1 - \mathbf{P}(S^{\min} \leq S_k \leq S^{\max}), \quad (7)$$

i.e. the probability of violation of the security interval.

The DAP is operated by a properly developed optimization algorithm which has the objective of maximizing the economic gain and simultaneously assuring that λ is lower than a predetermined maximal value λ_{\max} . The DAP program can be applied directly; however, a second possibility is proposed. Indeed, during the day, using updated short-term forecasts, it is possible to operate corrections to reduce the failure rate. This is realized by the HAP algorithm.

Both DAP and HAP algorithms use the technique introduced in [35] for providing PFR from BESSs. Therefore, before introducing DAP and HAP, the technique proposed in [35] is briefly recalled in the following.

A. Primary frequency regulation from BESS

Assume to have a BESS with capacity \tilde{E}_n which performs PFR with a droop coefficient α , and divide the time into windows of length T [h]. The energy required to provide PFR in the generic i -th time window $[iT, (i+1)T]$ is:

$$E_i^f = -\alpha \cdot \int_{iT}^{(i+1)T} \Delta f(t) dt = -\alpha W_i^f, \quad (8)$$

where W_i^f [Hz h] is defined as the integral over the current time interval of the frequency deviation. The analysis detailed in [35] demonstrates that a time series $\{W_i^f\}$ obtained from a large database of frequency measurements [40] and a given value of T (e.g. $T \in [1, 2, \dots, 24]$ h) can be modeled with an autoregressive (AR) process of order p [41]. This implies that:

$$W_{i+1}^f = \widehat{W}_{i+1}^f + \epsilon_{i+1}, \quad (9)$$

$$\widehat{W}_{i+1}^f = W_i^f \phi_1 + \dots + W_{i-p}^f \phi_p, \quad (10)$$

where $\{W_i^f, \dots, W_{i-p}^f\}$ are the measured value of the integral of the frequency deviation in the last p periods, $\{\phi_1, \dots, \phi_p\}$ are the AR coefficients defined by the analysis of the frequency database, \widehat{W}_i^f is the prediction W^f for the upcoming period, and ϵ_i is a zero-mean Gaussian random variable with standard deviation σ_T^w . The dependence on T of this standard deviation is explicitly indicated with the subscript because, in the following, different values of T will be used. It is worth remarking that σ_T^w increases with T .

Based on this model, the following *energy offset* is defined:

$$\widehat{E}_i^o = \left(S_i - \frac{1}{2} + \frac{\alpha \widehat{W}_i^f}{\tilde{E}_n} \right) \tilde{E}_n, \quad (11)$$

where S_i is the battery SOE at the beginning of the i -th time window. In [35] is proved that, if \widehat{E}_i^o is exchanged by the BESS during i -th time window, then the BESS can provide PFR with a maximal failure rate λ_{\max}^f , with respect the SOE the security interval $[0, 1]$, if the droop coefficient α is equal or lower than the maximal value

$$\alpha_{\max} = \frac{\tilde{E}_n}{2 \cdot \mu \cdot \sigma_T^w}, \quad (12)$$

where μ is $(1 - \lambda_{\max}^f/2)$ -th percentile of a zero-mean standard Gaussian random variable, which can be computed as $\mu = \sqrt{2} \operatorname{erf}^{-1}(1 - \lambda_{\max}^f)$.

B. Main requirements for PFR service

The integration of RES into grid regulating scheme requires the revision of the grid codes. In continental Europe, all the Transmission System Operators (TSOs) involved in the joint market IGCC have worked together to define pre-qualification and delivery rules for the BESSs which provide PCR [30]. In the UK, Nationalgrid (NGET) has developed the enhanced frequency response service and defined specific rules for the integration of the new resources into the markets [42]. In the United States of America, PJM has created another market in which the users are remunerated for the capacity, for the availability and for the performance in providing the service [28], [29].

By analyzing the mentioned documents, it results that the PFR markets are different each others and still changing, mainly because they are new. Therefore, the control strategy designed in this paper has the objective of matching the most important rules common between those markets rules:

- droop-based response to the frequency variations;
- the SOE must be kept within predefined limits;
- as requested by the market operators [30], [38], [42], a minimum PCR offer has to be ensured;
- according to some grid operators, the failure rate has to be kept lower than a maximal value (e.g. 5% in UK [29], [40]) or equal to zero [28], [30], [43], [44] in order not to pay penalties.

Finally note that the algorithm proposed in the present paper does not respect the capacity trading time line, *i.e.* the droop coefficient is computed daily and not weekly as in [30]. However, it is opinion of the authors that future markets deregulation will require to operate on shorter time windows in order to integrate all the new resources.

III. DAY-AHEAD PLANNING (DAP)

The DAP problem consists in the definition of the daily power delivery profile $\{P_k^m\}$ of the IS and the droop coefficient α , computed one day before. The objective is to maximize the economic gain, given set of available data and satisfying a set of technical constraints, as detailed in the following.

A. Available data

Given the time horizon $N = 24 \cdot 3600 / \tau$, the data supposed to be available at day $d - 1$ when the planning of day d is computed are:

- a PV forecast profile $\{\widehat{P}_k^{pv}\}_{k=0}^{N-1}$, with an associated confidence interval Δ_k^{pv} , such that $|P_k^{pv} - \widehat{P}_k^{pv}| \leq \Delta_k^{pv}$;
- the prediction of the frequency integral for the day-ahead \widehat{W}_d^f and the associated standard deviation σ_{24}^w , computed as described in Section II-A with $T = 24$ h;
- the energy price profile $\{c_k^e\}_{k=0}^{N-1}$;
- the PFR price c^f ;
- the day initial SOE, S_0 .

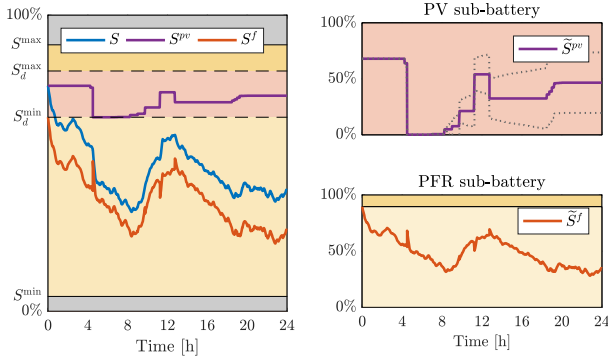


Fig. 2. DAP optimization principle scheme.

B. SOE constraints

Based on the PV forecast data, the PV power profile is represented with the following Gaussian model:

$$P_k^{pv} \sim \mathcal{N}(\hat{P}_k^{pv}, (\sigma_k^{pv})^2), \quad \sigma_k^{pv} = \Delta_k^{pv}/3 \quad (13)$$

so that $\mathbf{P}(|\hat{P}_k^{pv} - P_k^{pv}|) \leq 0.997$. From (5), (6) and definition (8) (with $T = \tau$) it follows that, for $k = 0 : N - 1$,

$$S_{k+1} = S_k - \frac{\tau(P_k^m - P_k^{pv})}{3600 \cdot E_n} + \frac{\alpha W_k^f}{E_n}. \quad (14)$$

Figure 2 shows the basic principle of the DAP optimization. Firstly, the equivalent BESS capacity E_n^s is defined as

$$E_n^s = E_n(S^{\max} - S^{\min}). \quad (15)$$

Then, each day, the quantities S_d^{\max} and S_d^{\min} are determined by the optimization, to divide E_n^s in two portions E_n^{pv} and E_n^f :

$$E_n^{pv} = E_n(S_d^{\max} - S_d^{\min}), \quad (16)$$

$$E_n^f = E_n^s - E_n^{pv}. \quad (17)$$

It is obviously required that

$$S^{\min} \leq S_d^{\min} \leq S_d^{\max} \leq S^{\max}. \quad (18)$$

The idea is to use the portion E_n^{pv} to correct the PV prediction errors, and the portion E_n^f to provide PFR, as they were two different batteries: the *PV battery* and the *PFR battery*, respectively. Two equivalent SOE trajectories $\{\tilde{S}_k^{pv}\}$ and $\{\tilde{S}_k^f\}$ are supposed to move in these two batteries. They are defined in *p.u.* with respect to the two capacities E_n^{pv} and E_n^f (right plots in Fig. 2), by the following dynamical equations (with $k = 0 : N - 1$):

$$\tilde{S}_{k+1}^{pv} = \tilde{S}_k^{pv} - \frac{\tau(P_k^m - P_k^{pv})}{3600 \cdot E_n^{pv}} \quad (19)$$

$$\tilde{S}_0^{pv} = \frac{E_n(S_0 - S_d^{\min})}{E_n^{pv}}, \quad (20)$$

$$\tilde{S}_{k+1}^f = \tilde{S}_k^f + \frac{\alpha W_k^f}{E_n^f}, \quad (21)$$

$$\tilde{S}_0^f = \frac{E_n(S_d^{\min} - S^{\min})}{E_n^f}, \quad (22)$$

It can be proved by induction that, for $k = 0 : N$,

$$S_k = S_k^{pv} + (S_k^f - S_d^{\min}), \quad (23)$$

where S_k^f and S_k^{pv} are defined as it follows (see the left plots in Fig. 2 for an example):

$$S_k^{pv} = \frac{E_n^{pv} \tilde{S}_k^{pv}}{E_n} + S_d^{\min}, \quad S_k^f = \frac{E_n^f \tilde{S}_k^f}{E_n} + S^{\min}. \quad (24)$$

The component S^{pv} is driven by the dispatch power P^m and the PV power P^{pv} , whereas the component S^f is driven by the frequency variations. Since the (local) PV production and grid frequency can be assumed to be statistically independent, also S^{pv} and S^f result to be independent. This implies the following result, which is proved in the appendix section.

Proposition 1: If, for all $k = 0 : N$,

$$\mathbf{P}(0 \leq \tilde{S}_k^{pv} \leq 1) \geq 1 - \beta, \quad (25)$$

$$\mathbf{P}(0 \leq \tilde{S}_k^f \leq 1) = 1 - \lambda_{\max}^f, \quad (26)$$

then

$$\mathbf{P}(S^{\min} \leq S_k \leq S^{\max}) \geq 1 - \lambda_{\max} \quad (27)$$

with

$$\lambda_{\max} = \lambda_{\max}^f + \beta - \lambda_{\max}^f \beta. \quad (28)$$

This proposition means that if (25) and (26) hold true, than λ_{\max} is the resulting maximal failure rate of the IS.

Relation (25) is considered as a chance constraint. Using the Gaussian representation (13), assuming that the PV prediction errors and the battery modelling errors are independent, and that the sampling time τ is large enough to suppose that the PV prediction errors at different time steps are mutually independent, from (19)–(20), it follows that, for $k = 0 : N$,

$$\tilde{S}_k^{pv} \sim \mathcal{N}(m_k^s, (\sigma_k^s)^2), \quad (29)$$

where

$$m_k^s = \tilde{S}_0^{pv} - \frac{\tau}{3600 \cdot E_n^{pv}} \sum_{j=0}^{k-1} (P_j^m - \hat{P}_j^{pv}), \quad (30)$$

$$(\sigma_k^s)^2 = \left(\frac{\tau}{3600 \cdot E_n^{pv}} \right)^2 \cdot \sum_{j=0}^{k-1} (\sigma_j^{pv})^2 \quad (31)$$

To obtain (25), the following separated chance constraints are defined, for all $k = 0 : N$:

$$\mathbf{P}(\tilde{S}_k^{pv} \leq 1) \geq 1 - \frac{\beta}{2}, \quad \mathbf{P}(\tilde{S}_k^{pv} \geq 0) \geq 1 - \frac{\beta}{2} \quad (32)$$

which, using the Gaussian model (29)–(31), can be expressed with the equivalent deterministic constraints (see [37] or [14] for details):

$$m_k^s + \theta_s \sigma_k^s \leq 1, \quad (33)$$

$$-m_k^s + \theta_s \sigma_k^s \leq 0, \quad (34)$$

where $\theta_s = \sqrt{2} \text{erf}^{-1}(1 - \beta)$.

To obtain (26), the method recalled in Section II-A is applied to the PFR battery considering a period $T = 24$ h. Recall that S_d^{\min} and S_d^{\max} are defined by the DAP optimization. Considering (22), this implies that the initial condition \tilde{S}_0^f , at the beginning of the day, is defined by the optimization. Therefore, by (11), if

$$\tilde{S}_0^f = \frac{1}{2} - \frac{\alpha \hat{W}_d^f}{E_n^f}, \quad (35)$$

then the required energy offset $\widehat{E}_d^o = 0$, and therefore satisfied with α given by

$$\alpha = \frac{E_n^f}{2\mu\sigma_{24}^w}.$$

Using the definition of E_n^f in (17) and the relation (18), it can be shown that (35) and (36) are equivalent to

$$\begin{aligned} 2\alpha\widehat{W}_d^f &= E_n[(S_d^{\max} + S_d^{\min}) - (S_d^{\max} + S_d^{\min})] \\ 2\alpha\mu\sigma_{24}^w &= E_n[(S_d^{\max} - S_d^{\min}) - (S_d^{\max} - S_d^{\min})]. \end{aligned} \quad (38)$$

C. Power constraints

As defined in Section II, the BESS power is limited by the nominal value P_n^b . From (5), it results that the following inequality should be always satisfied:

$$|P^b| = |P^m - P^{pv} - \alpha\Delta f| \leq P_n^b. \quad (39)$$

Since it is assumed that, for $k = 0 : N - 1$,

$$0 \leq P_k^m \leq P_n^t \quad (40)$$

and $P_k^{pv} \geq 0$ by definition, then, for the day-ahead d , there are two worst cases, which are covered with the following chance constraints (with $k = 0 : N - 1$):

$$\mathbf{P}(P_k^m - P_k^{pv} + \alpha\Delta f^{\max} \leq P_n^b) \geq 1 - \gamma, \quad (41)$$

$$\mathbf{P}(P_k^m - P_k^{pv} - \alpha\Delta f^{\max} \geq -P_n^b) \geq 1 - \gamma. \quad (42)$$

where Δf^{\max} is the maximal frequency variation [4]. Based on the Gaussian model of the PV forecasts (13), (41) and (42) can be expressed with the equivalent deterministic constraints (see [37] or [14] for details):

$$P_k^m - \hat{P}_k^{pv} + \alpha\Delta f_{\max} + \theta_b\sigma_k^{pv} \leq P_n^b, \quad (43)$$

$$P_k^m - \hat{P}_k^{pv} - \alpha\Delta f_{\max} - \theta_b\sigma_k^{pv} \geq -P_n^b, \quad (44)$$

with $k = 0 : N - 1$, and $\theta_b = \sqrt{2}\text{erf}^{-1}(1 - 2\gamma)$.

D. Smoothness constraints

Two additional constraints are defined to limit the variations of P^m and m_k^s between consecutive set-points time steps, for $k = 0 : N - 1$,

$$|P_{k+1}^m - P_k^m| \leq \Delta P_{\max}^m, \quad (45)$$

$$|m_{k+1}^s - m_k^s| \leq \Delta m_{\max}^s. \quad (46)$$

E. The DAP algorithm

Given a desired maximal failure rate λ_{\max} , the DAP algorithm consists in the solution of the following linear optimization problem:

$$\begin{aligned} J^* &= \max_{\{P_k^m\}, \alpha, S_d^{\min}, S_d^{\max}} \sum_{k=0}^{N-1} c_k^e \tau P_k^m + c^f \alpha \\ &\text{subject to (3), (15)–(18), (20), (30)–(31), (33)–(34),} \\ &\quad \text{(37)–(38), (40), (43)–(44), (45)–(46)} \end{aligned}$$

The result of the optimization are the optimal IS base power profile $\{P_k^{md}\} = \{P_k^{m*}\}$ and the droop coefficient $\alpha^d = \alpha^*$, both defined the day before the delivery. The value of the cost function J^* is equal to the day-ahead economical gain.

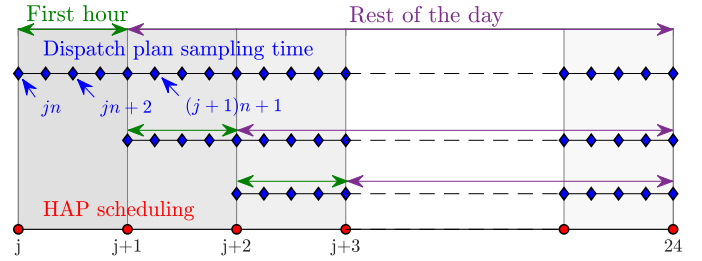


Fig. 3. HAP time scheduling.

IV. HOURS-AHEAD PLANNING (HAP)

The hour-ahead planning is a lower level controller which is re-computed every hour within the delivery day. The HAP routine receives from the DAP one the power delivery plan $\{P_k^{md}\}$ and the droop coefficient α^d . The objective of HAP is to correct the plan $\{P_k^{md}\}$ to guarantee the provision of PFR, keeping the droop coefficient α^d and reducing the expected DAP failure rate λ_{\max} to a lower value λ'_{\max} , always maximizing the economical income.

Figure 3 shows the HAP time scheduling. Let $j = 0, 1, \dots, 23$ indicate the hours during the day, and $n = 3600/\tau$ be the number of intra-hour power set-points defined according to the dispatch plan sampling time. Moreover, let $N_j = N - j \cdot n$ be the number of power set-points remaining from the j -th hour to the end of the day.

At the beginning of hour j , the IS power profile $\{P_k^m\}$ with $k = jn : N - 1$ is re-programmed. Then, only the first n steps, corresponding to the first hour of the dispatch plan, are applied. At hour $j+1$, the HAP optimization is repeated. This time scheduling can be called *reducing horizon*, and, similarly to the *receding horizon* principle adopted by Model Predictive Control (MPC), it allows the control algorithm to be more robust with respect to modelling errors. In particular, at each hour, updated, and thus more accurate, PV generation and PFR energy requirement forecasts may be available, as well as the current value of the battery SOE. These updated data are useful to suitably correct the DAP program.

Based on this idea, as shown in Fig. 3, the time from hour j to the end of the day, is divided into two phases: the First Hour (FH) ($k = jn : (j+1)n$), and the remaining time from hour $j+1$ to the end of the day ($k = (j+1)n : N$), from now named Rest of the Day (RoD).

At hour j , the available data are:

- the DAP power profile $\{P_k^{md}\}$, $k = j \cdot n : N - 1$ traded at the energy market;
- the droop coefficient α^d , defined for a given failure rate λ^d , to be guaranteed during all the day;
- the updated PV forecasts $\{\hat{P}_k^{pv}\}$, with the associated standard deviations σ_k^{pv} , $k = j \cdot n : N - 1$ (using the same the Gaussian model (13) adopted for DAP);
- the prediction of the frequency integral for the first hour \widehat{W}_h^f and the associated standard deviation σ_1^w , computed as described in Section II-A with $T = 1$ h;
- the prediction of the frequency integral for the rest of the day \widehat{W}_r^f and the associated standard deviation σ_{23-j}^w , computed as described in Section II-A with $T = 23 - j$ h;

- g) the penalty cost profile $\{c_k^p\}$, $k = j \cdot n : N - 1$ to be paid for a difference of the energy effectively exported by the IS from the energy traded at the day-ahead market;
- h) the intra-day energy price profile $\{c_k^i\}$, $k = j \cdot n : N - 1$;
- i) the current battery SOE, S_{jn} .

For both the time windows FH and RoD, an approach similar to DAP is adopted. In particular, the basic idea of the partition of the BESS capacity by the definition of the thresholds S_d^{\max} and S_d^{\min} is re-applied with the definition of different thresholds: S_h^{\max} , S_h^{\min} , for the FH, and S_r^{\max} , S_r^{\min} , for the RoD. The partition into two time windows is adopted in order to give more degrees of freedom to the optimization for the FH. Thanks to the use of short-term, and thus more accurate, predictions, the optimization over the FH will be finer. It is worth remarking that, as mentioned before, at each hour, the optimization results are applied only for the FH.

The HAP optimization problem, solved at each hour j , is formulated as it follows.

$$\begin{aligned} & \max_{\{P_k^m\}, \mu_h, \mu_r} L_j \\ L_j = & \sum_{k=jn}^{N-1} (c_k^i - c_k^p) \tau (P_k^m - P_k^{md}) \delta_k^+ - c_k^p \tau (P_k^m - P_k^{md}) \delta_k^- \\ & + w_h \mu_h + w_r \mu_r \end{aligned} \quad (47)$$

subject to:

$$S^{\min} \leq S_h^{\min} \leq S_h^{\max} \leq S^{\max}, \quad (48)$$

$$m_k^s + \theta_h \sigma_k^s \leq S_h^{\max} \quad \text{for } k = jn : j(n+1), \quad (49)$$

$$-m_k^s + \theta_h \sigma_k^s \leq S_h^{\min} \quad \text{for } k = jn : j(n+1), \quad (50)$$

$$2\alpha^d \widehat{W}_h^f = E_n[(S^{\max} + S^{\min}) - (S_h^{\max} + S_h^{\min})], \quad (51)$$

$$2\alpha^d \mu_h \sigma_{24}^w = E_n[(S^{\max} - S^{\min}) - (S_h^{\max} - S_h^{\min})], \quad (52)$$

$$\mu \leq \mu_h \leq \mu_{\max}, \quad (53)$$

$$S^{\min} \leq S_r^{\min} \leq S_r^{\max} \leq S^{\max}, \quad (54)$$

$$m_k^s + \theta_r \sigma_k^s \leq S_r^{\max} \quad \text{for } k = j(n+1) : N, \quad (55)$$

$$-m_k^s + \theta_r \sigma_k^s \leq S_r^{\min} \quad \text{for } k = j(n+1) : N, \quad (56)$$

$$2\alpha^d \widehat{W}_r^f = E_n[(S^{\max} + S^{\min}) - (S_r^{\max} + S_r^{\min})], \quad (57)$$

$$2\alpha^d \mu_r \sigma_{24}^w = E_n[(S^{\max} - S^{\min}) - (S_r^{\max} - S_r^{\min})], \quad (58)$$

$$\mu \leq \mu_r \leq \mu_{\max}, \quad (59)$$

$$m_k^s = S_{jn} - \frac{\tau}{3600 \cdot E_n} \sum_{i=jn}^{k-1} (P_i^m - \widehat{P}_i^{pv}), \quad (60)$$

$$(\sigma_k^s)^2 = \left(\frac{\tau}{3600 \cdot E_n} \right)^2 \cdot \sum_{i=jn}^{k-1} (\sigma_i^{pv})^2, \quad (61)$$

$$P_k^m - \widehat{P}_k^{pv} + \alpha^d \Delta f_{\max} + \theta_b \sigma_k^{pv} \leq P_n^b \quad (62)$$

$$P_k^m - \widehat{P}_k^{pv} - \alpha^d \Delta f_{\max} - \theta_b \sigma_k^{pv} \geq -P_n^b, \quad (63)$$

$$0 \leq P_k^m \leq P_n^t, \quad (64)$$

$$|P_{k+1}^m - P_k^m| \leq \Delta P_{\max}^m, \quad (65)$$

$$|m_{k+1}^s - m_k^s| \leq \Delta m_{\max}^s. \quad (66)$$

The optimization problem results to be mixed-integer with linear constraints. Indeed, there are two binary variables: δ_k^+ defined (through additive linear constraints not reported for

clarity of presentation) to be equal to 1 when $P_k^m \geq P_k^{md}$ and 0 otherwise, and $\delta_k^- = 1 - \delta_k^+$.

For each of the two time windows, starting from the definitions of the new thresholds S_h^{\max} and S_h^{\min} , for the FH, and S_r^{\max} and S_r^{\min} for the RoD, the SOE constraints defined for HAP are reformulated as in (48)–(61).

Let us focus on constraints (51)–(52) and (57)–(58). They are the reformulation of the DAP constraints (37)–(38), for the FH and the RoD, respectively. In DAP, (37)–(38) have to be respected in order to assure the maximal failure rate λ_{\max}^f due to PFR, which is related to coefficient μ by the relation $\mu = \sqrt{2} \text{erf}^{-1}(1 - \lambda_{\max}^f)$ (see Section II-A). It can be easily shown that μ increases when λ_{\max}^f decreases. Therefore, if (37)–(38) are satisfied with a $\bar{\mu} \geq \mu$, the maximal failure rate λ_{\max} is reduced. Indeed, by (28) λ_{\max} results to be reduced if λ_{\max}^f decreases. Constraints (51)–(52) for the FH and (57)–(58) for the RoD, are therefore re-formulated using the relevant predictions \widehat{W}_h^f and \widehat{W}_r^f and imposing that the droop coefficient α is equal to α^d , computed by the DAP.

Two optimization variables μ_h and μ_r , are introduced for the FH and RoD time-windows. The cost function (47) is designed in order to increase their values, in order to obtain the reduction of the failure rate. With constraints (53) and (59), μ_h and μ_r are limited by the minimal value μ , which gives the guaranty to obtain the DAP failure rate λ_{\max}^f , and by the maximal value $\mu_{\max} = \sqrt{2} \text{erf}^{-1}(1 - \bar{\lambda}_{\max}^f)$, corresponding to the maximal reduced failure rate $\bar{\lambda}_{\max}^f < \lambda_{\max}^f$. The power and smoothness constraints (62)–(66) are re-written, as in DAP, for the entire interval $k = jn : N - 1$, with $\alpha = \alpha^d$.

The cost function (47) considers both the economical gain, determined by the balance between penalties and intra-day energy prices, and the reduction of the DAP failure rate, which, as mentioned, corresponds to the maximization of the coefficients μ_h and μ_r . The optimization weights w_h and w_r have a different unit from the costs c^p and c^e . Therefore, they has to be suitably normalized. It is worth remarking that the minimization of the failure rate may be in contrast with the maximization of the economical income. Therefore, the sizing of the weights w_h and w_r defines the priority level between the quality of the PFR service and the economical gain.

V. SIMULATION RESULTS

A set of simulations has been performed considering real markets' data. The Italian day-ahead (MGP) and intra-day market (MI2) results (February 2019) [45] has been selected as input of DAP and HAP problems, respectively. The penalty for the variations on the dispatched power is fixed to 0.05€ kWh^{-1} . Moreover, the frequency regulating capacity price has been selected from the the results of the International PCR markets between August 2018 and March 2019 [30].

DAP and HAP algorithms have been implemented in MATLAB/Simulink, and optimization problems have been written using the General Algebraic Modelling System (GAMS) language and solved with CPLEX. Battery is modelled with a standard equivalent circuit in which the internal resistance is a function of the SOE and of the electromotive force. Thus, a variable nonunitary battery efficiency has been implemented.

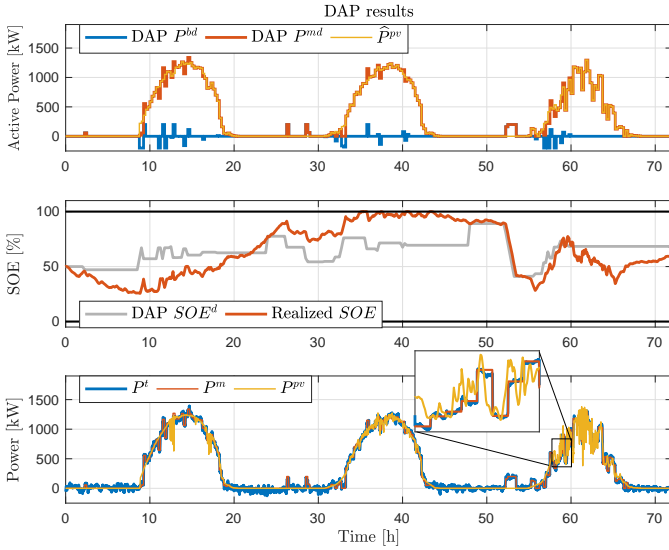


Fig. 4. Simulation results for the DAP only configuration, Case A: 1500 kW PV, 500 kWh BESS. Top: planning power profiles; middle: planned and realized SOE profiles; bottom: realized power profiles.

Inputs of the simulator are real PV measurements and PV forecasts registered in the low-voltage (LV) microgrid realized by the University of Genova [46]. Moreover frequency measurements from the UK grid has been adopted in the construction of the AR models and for the simulations [40].

Simulations have been executed over a 21 days period and considering the implementation only of DAP, and of both DAP and HAP. Moreover, five different cases are proposed characterized by different PV-BESS sizes, as reported in Table I. Considering devices rating, the ISMS is expected to differently balance the two services, *i.e.* a larger BESS will provide higher regulating capacity but can rely on smaller offsets for charge management, on the other hand, a large PV will drive the ISMS to privilege the dispatch service.

Table II shows the parameters adopted for the IS. Among the others: the minimum droop coefficient α_{\min} is defined according to (3) with respect to the PV nominal power, with an equivalent maximal stastism b_p^{\max} fixed to 8% [38]; the maximum failure rate λ_{\max} is fixed at 5%, according for example to the requirements of the UK market [29], [40]; the dispatch sampling time τ is set to 15 min according to the Italian energy market [45].

Figure 4 shows a section of the simulation of the stand alone DAP controller. The top plot reports the dispatch plan $\{P_k^{md}\}$, the day ahead PV forecast $\{\hat{P}_k^{pv}\}$ and the battery offset program $\{P_k^{bd}\} = \{P_k^{md} - \hat{P}_k^{pv}\}$. The middle plot depicts the programmed SOE trajectory and the realized ones. While the bottom plot shows the resulting profiles of the total power at the GCP P^t , of the base dispatch power P^m and of the PV generation P^{pv} .

The detailed numerical results of all the simulations in the the stand alone DAP case are reported in Table I. The reported data show that the DAP is able to determine a reliable power profile, which allows the IS to perform both the services with a failure rate lower than the prescribed maximal value $\lambda_{\max} = 5\%$.

TABLE I
SIMULATION RESULTS.

Case	λ %	Total €	PCR €	Dispatch €	Penalty €
A	0.424	27798	15756	12042	0
	0	24825	14483	11363	-1020
B	0.530	35949	23940	12010	0
	0	32150	22575	11059	-1484
C	0.403	38765	14420	24345	0
	0	36997	14035	23797	-835
D	0.234	41536	4821	36714	0
	0	40897	4957	36426	-486
E	0.941	41104	4274	36830	0
	0	40451	4287	36580	-416

Resources sizes: A. PV 500 kW, BESS 1500 kW; B. PV 500 kW, BESS 1000 kW; C. PV 1000 kW, BESS 1000 kW; D. PV 1500 kW, BESS 500 kW; E. PV 1500 kW, BESS 320 kW.

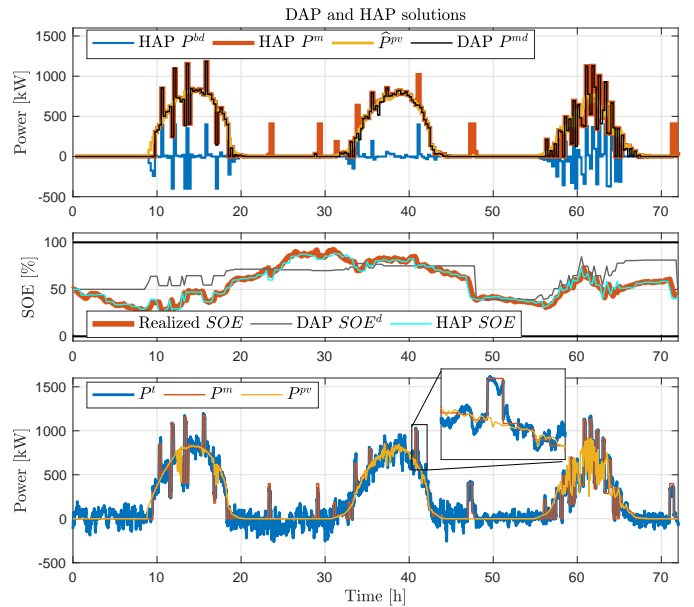


Fig. 5. Simulation results for the DAP-HAP configuration, Case C: 1000 kW PV, 1000 kWh BESS. Top: planning power profiles; middle: planned and realized SOE profiles; bottom: realized power profiles.

Figure 5 shows an example of the results obtained with the DAP-HAP configuration. In particular, in the top plot the modification operated by HAP with respect to DAP can be appreciated. For example, during the night operations (from hour 20 to hour 31) the HAP commands some short power delivery in order to discharge the battery and avoid to reach the full charge condition. Also Fig. 6 makes evidence on the advantages on using the HAP procedure. Indeed, with the stand alone DAP, during the first 50 hours, the battery SOE reaches the up limit (failure), whereas this does not happen when HAP is used. It can be observed that in all the considered cases the DAP-HAP strategy allows obtaining a null failure rate, as shown in Table I. It is worth remarking that one of objective of the HAP is to reduce the expect failure rate to a value below 1%.

TABLE II
SIMULATION PARAMETERS.

Variable	Description	Value
τ	Dispatch sampling time	15 min
ΔP_{\max}^m	Maximal power deviation	40% P_n^t
Δm_{\max}^s	Maximal SOE deviation	10%
γ	Battery power chance-constraints coefficient	1%
β	Battery SOE chance-constraints coefficient	1%
α_{\min}	Minimal droop coefficient as (4) with b_p^{\max} 8%	-
α_{\max}	Maximal droop coefficient	inf
S^{\min}	Maximal battery SOE	100%
S^{\max}	Maximal battery SOE	0%
Δf^{\max}	Maximal frequency deviation	0.2 Hz
μ	Equivalent to DAP failure rate $\lambda_{\max} = 5\%$	1.96
$\bar{\mu}_{\max}$	Equivalent to HAP failure rate $\bar{\lambda}_{\max} = 0.3\%$	3

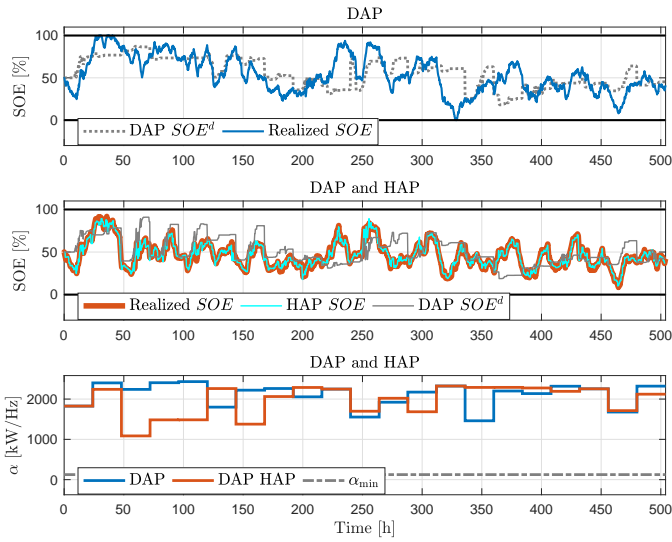


Fig. 6. Simulation results for the DAP only and DAP-HAP configurations, Case D: 500 kW PV, 1500 kWh BESS. Top: planned and realized SOE profiles in the stand alone DAP configuration; middle: planned and realized SOE profiles in the DAP-HAP configuration; bottom: droop coefficients obtained in the DAP only and DAP-HAP configurations.

The bottom plot of Fig. 6 reports the droop coefficients computed with the two configurations. They result to be comparable, even if the DAP solution allows to reach slightly higher values. As a consequence, the total economical income results to be higher. It is worth remarking that this results are not affected by some penalty that could be paid for reaching fail conditions in the HAP case.

The results reported in Table I prove the effectiveness of the control algorithms with all the different considered configurations. All cases use the same price vectors, therefore, the power ratings of the IS has a relevance on the total income. Increasing the PV power rating allows to reach higher income from the dispatch, while the highest regulating capacities are obtained with larger BESSs.

It is finally worth remarking that, as noticed in Section II, the control algorithms consider a battery with unitary efficiency. On the contrary, the test battery model adopted for the

tests account for the efficiency. Such a model has been derived from the simulation setup presented and validated in [35], [39]. The model consists in the series of an internal voltage source and of variable resistance, the parameters obtained from measurements the original grid-scale lithium-titanate battery rated 560 kWh [47] has been scaled to match the different battery sizes simulated. The obtained results prove that such an approximation in the control design does not influence the overall performance.

VI. CONCLUSIONS

This paper presents a strategy for the optimal planning of an integrated BESS-PV system, which provides frequency regulation and generation dispatch. The control architecture is composed by two algorithms. The first one, DAP, is executed the day before the delivery and defines the power dispatch plan and a droop coefficient for the PFR, on the basis of PV forecasts and predictions of the energy required for providing PFR. The delivery day, at each hour, the second algorithm, named HAP, is executed in order to allow the IS to perform its tasks in a continuous and reliable way by using updated short-term forecasts. The two algorithms are designed to maximize the total incomes and the performance in providing PFR. They use chance-constrained optimization in order to model the forecasts errors. The control framework has been validated by simulations. Future works will consider different applications using a similar approach, also non-Gaussian representations of uncertainties and stochastic models of the energy prices.

APPENDIX A

PROOF OF PROPOSITION 1

Using (24), from (25) and (26), it follows that

$$\mathbf{P}\left(0 \leq S_k^{pv} - S_d^{\min} \leq \frac{E_n^{pv}}{E_n}\right) = \mathbf{P}(A) \geq 1 - \beta,$$

$$\mathbf{P}\left(0 \leq S_k^f - S^{\min} \leq \frac{E_n^f}{E_n}\right) = \mathbf{P}(B) = 1 - \lambda_{\max}^f,$$

where, A and B indicate the two considered constraints. Since S_k^{pv} and S_k^f are independent, it results that

$$\mathbf{P}(A \cap B) = \mathbf{P}(A) \cdot \mathbf{P}(B) = (1 - \beta) \cdot (1 - \lambda_{\max}^f) = 1 - \lambda_{\max}$$

where λ_{\max} is equal to the one defined in (28). Now consider that, because of elementary set inclusion properties,

$$\begin{aligned} \mathbf{P}\left(0 \leq S_k^{pv} + S_k^f - S_d^{\min} - S^{\max} \leq \frac{E_n^{pv}}{E_n} + \frac{E_n^f}{E_n}\right) \\ \geq \mathbf{P}(A \cap B) \geq 1 - \lambda_{\max} \end{aligned}$$

from which, taking into account (23), it follows that

$$\mathbf{P}\left(0 \leq S_k - S^{\min} \leq \frac{E_n^{pv} + E_n^f}{E_n}\right) \geq 1 - \lambda_{\max}$$

and, therefore,

$$\mathbf{P}\left(S^{\min} \leq S_k \leq \frac{E_n^{pv} + E_n^f}{E_n} + S^{\min}\right) \geq 1 - \lambda_{\max}.$$

To conclude, (27) is proved by noticing that from the definitions (16) and (17) it results that

$$\frac{E_n^{pv} + E_n^f}{E_n} + S^{\min} = \frac{E_n^s}{E_n} + S^{\min} = S^{\max}.$$

REFERENCES

- [1] H. Ye, W. Pei, and Z. Qi, "Analytical modeling of inertial and droop responses from a wind farm for short-term frequency regulation in power systems," *IEEE Trans. Power Syst.*, vol. 31, no. 5, pp. 3414–3423, Sep. 2016.
- [2] E. Vrettos and G. Andersson, "Scheduling and provision of secondary frequency reserves by aggregations of commercial buildings," *IEEE Trans. Sustain. Energy*, vol. 7, no. 2, pp. 850–864, April 2016.
- [3] F. Baccino, F. Conte, S. Massucco, F. Silvestro, and S. Grillo, "Frequency regulation by management of building cooling systems through model predictive control," in *Power Syst. Comput. Conf. (PSCC)*, 2014.
- [4] UCTE, "Appendix 1, load-frequency control and performance," Operation Handbook, Dec. 2009.
- [5] Y. Guo and Y. Fang, "Electricity cost saving strategy in data centers by using energy storage," *IEEE Trans. Parallel Distrib. Syst.*, vol. 24, no. 6, pp. 1149–1160, 2013.
- [6] Y. Wang, B. Wang, C.-C. Chu, H. Pota, and R. Gadh, "Energy management for a commercial building microgrid with stationary and mobile battery storage," *Energy and Buildings*, vol. 116, pp. 141–150, 2016.
- [7] N.-K. C. Nair and N. Garimella, "Battery energy storage systems: Assessment for small-scale renewable energy integration," *Energy and Buildings*, vol. 42, no. 11, pp. 2124–2130, 2010.
- [8] B. Wasowicz, S. Koopmann, T. Dederichs, A. Schnettler, and U. Spaetling, "Evaluating regulatory and market frameworks for energy storage deployment in electricity grids with high renewable energy penetration," in *9th Int. Conf. on the European Energy Market (EEM)*, 2012.
- [9] E. Namor, F. Sossan, R. Cherkaoui, and M. Paolone, "Control of battery storage systems for the simultaneous provision of multiple services," *IEEE Trans. Smart Grid*, vol. 10, no. 3, pp. 2799–2808, May 2019.
- [10] A. Oudalov, R. Cherkaoui, and A. Beguin, "Sizing and optimal operation of battery energy storage system for peak shaving application," in *IEEE PowerTech*, 2007, pp. 621–625.
- [11] K. Christakou, D.-C. Tomozei, M. Bahrampianah, J.-Y. Le Boudec, and M. Paolone, "Primary voltage control in active distribution networks via broadcast signals: The case of distributed storage," *IEEE Trans. Smart Grid*, vol. 5, no. 5, pp. 2314–2325, 2014.
- [12] A. Oudalov, D. Chartouni, and C. Ohler, "Optimizing a battery energy storage system for primary frequency control," *IEEE Trans. Power Syst.*, vol. 22, no. 3, pp. 1259–1266, 2007.
- [13] E. Bullich-Massagué, M. Aragüés-Peñalba, A. Sumper, and O. Boix-Aragones, "Active power control in a hybrid pv-storage power plant for frequency support," *Solar Energy*, vol. 144, pp. 49–62, 2017.
- [14] F. Conte, S. Massucco, M. Saviozzi, and F. Silvestro, "A stochastic optimization method for planning and real-time control of integrated pv-storage systems: Design and experimental validation," *IEEE Trans. Sustain. Energy*, vol. 9, no. 3, pp. 1188–1197, July 2018.
- [15] F. Silvestro, F. Conte, F. D'Agostino, P. Pongiglione, and M. Saviozzi, "Mixed-integer algorithm for optimal dispatch of integrated PV-storage systems," *IEEE Trans. Ind. Appl.*, vol. 55, no. 1, pp. 238–247, Jan. 2019.
- [16] Y. Yang, Q. Ye, L. J. Tung, M. Greenleaf, and H. Li, "Integrated size and energy management design of battery storage to enhance grid integration of large-scale PV power plants," *IEEE Trans. Ind. Electron.*, vol. 65, no. 1, pp. 394–402, Jan. 2018.
- [17] X. Li, D. Hui, and X. Lai, "Battery energy storage station (BESS)-based smoothing control of photovoltaic (PV) and wind power generation fluctuations," *IEEE Trans. Sustain. Energy*, vol. 4, no. 2, pp. 464–473, April 2013.
- [18] M. T. Lawder, B. Suthar, P. W. C. Northrop, S. De, C. M. Hoff, O. Leitermann, M. L. Crow, S. Santhanagopalan, and V. R. Subramanian, "Battery energy storage system (BESS) and battery management system (BMS) for grid-scale applications," *Proceedings of the IEEE*, vol. 102, no. 6, pp. 1014–1030, June 2014.
- [19] V. Zamani, A. Cortés, J. Kleissl, and S. Martínez, "Integration of PV generation and storage on power distribution systems using MPC," in *2015 IEEE Power Energy Society General Meeting*, July 2015.
- [20] A. Park and P. Lappas, "Evaluating demand charge reduction for commercial-scale solar PV coupled with battery storage," *Renewable Energy*, vol. 108, pp. 523–532, 2017.
- [21] E. Stai, L. Reyes-Chamorro, F. Sossan, J. Le Boudec, and M. Paolone, "Dispatching stochastic heterogeneous resources accounting for grid and battery losses," *IEEE Trans. Smart Grid*, vol. 9, no. 6, pp. 6522–6539, Nov. 2018.
- [22] E. Mohagheghi, A. Gabash, M. Alramlawi, and P. Li, "Real-time optimal power flow with reactive power dispatch of wind stations using a reconciliation algorithm," *Renewable Energy*, vol. 126, pp. 509–523, 2018.
- [23] E. Mohagheghi, M. Alramlawi, A. Gabash, and P. Li, "A survey of real-time optimal power flow," *Energies*, vol. 11, no. 11, p. 3142, 2018.
- [24] X. Lu, K. Sun, J. M. Guerrero, J. C. Vasquez, and L. Huang, "State-of-charge balance using adaptive droop control for distributed energy storage systems in dc microgrid applications," *IEEE Trans. Ind. Electron.*, vol. 61, no. 6, pp. 2804–2815, 2014.
- [25] O. Mégel, J. L. Mathieu, and G. Andersson, "Maximizing the potential of energy storage to provide fast frequency control," in *IEEE ISGT Europe*, 2013.
- [26] M. Khalid and A. V. Savkin, "Model predictive control based efficient operation of battery energy storage system for primary frequency control," in *Int. Conf. on Contr. Autom. Robotics & Vision (ICARCV)*, 2010.
- [27] *PJM Manual 12: Balancing Operations*, 39th ed., PJM, Feb. 2019.
- [28] *PJM Manual 18: PJM Capacity Market*, 41st ed., PJM, Jan. 2019.
- [29] *Enhanced frequency response: invitation to tender for pre-qualified parties*, 8th ed., Nationalgrid, July 2016.
- [30] "Regelleistung.net: International primary control reserve tender overview," <https://www.regelleistung.net>, accessed on March 2019.
- [31] Y. Shi, B. Xu, D. Wang, and B. Zhang, "Using battery storage for peak shaving and frequency regulation: Joint optimization for superlinear gains," in *2018 IEEE Power Energy Society General Meeting (PESGM)*, Aug. 2018.
- [32] A. Perez, R. Moreno, R. Moreira, M. Orchard, and G. Strbac, "Effect of battery degradation on multi-service portfolios of energy storage," *IEEE Transactions on Sustainable Energy*, vol. 7, no. 4, pp. 1718–1729, Oct. 2016.
- [33] J. Eyer and G. Corey, "Energy storage for the electricity grid: Benefits and market potential assessment guide," *Sandia National Laboratories*, vol. 20, no. 10, p. 5, 2010.
- [34] B. Cheng and W. B. Powell, "Co-optimizing battery storage for the frequency regulation and energy arbitrage using multi-scale dynamic programming," *IEEE Transactions on Smart Grid*, vol. 9, no. 3, pp. 1997–2005, May 2018.
- [35] G.-P. Schiapparelli, E. Namor, F. Sossan, R. Cherkaoui, S. Massucco, and M. Paolone, "Quantification of primary frequency control provision from battery energy storage systems connected to active distribution networks," in *2018 Power Systems Computation Conference (PSCC)*, June 2018.
- [36] A. Borghetti, M. Bosetti, S. Grillo, A. Morini, M. Paolone, and F. Silvestro, "A two-stage scheduler of distributed energy resources," in *IEEE PowerTech*, 2007, pp. 2168–2173.
- [37] E. Cinquemani, M. Agarwal, D. Chatterjee, and J. Lygeros, "Convexity and convex approximations of discrete-time stochastic control problems with constraints," *Automatica*, vol. 47, no. 9, pp. 2082–2087, 2011.
- [38] *ENTSO-e network code for requirements for grid connection applicable to all generators*, ENTSO-E AISBL: Brussels, Belgium, 2012.
- [39] F. Conte, S. Massucco, G. P. Schiapparelli, and F. Silvestro, "Frequency regulation services by a bess-generator system using predictive control," in *2019 IEEE Milan PowerTech*, June 2019.
- [40] "Enhanced frequency response, national grid electricity transmission. downloaded on april 24th, 2017." [Online]. Available: <http://www2.nationalgrid.com/Enhanced-Frequency-Response.aspx>
- [41] H. Madsen, *Time Series Analysis*, ser. Chapman & Hall/CRC Texts in Statistical Science. Taylor & Francis, 2007.
- [42] V. Pandurangan, H. Zareipour, and O. Malik, "Frequency regulation services: A comparative study of select north american and european reserve markets," in *2012 North American Power Symposium (NAPS)*, Sep. 2012.
- [43] *Basic principles of ancillary service products*, Swissgrid, Feb. 2017. [Online]. Available: www.swissgrid.ch
- [44] A. Zeh, M. Müller, M. Naumann, H. Hesse, A. Jossen, and R. Witzmann, "Fundamentals of using battery energy storage systems to provide primary control reserves in germany," *Batteries*, vol. 2, no. 3, p. 29, 2016.
- [45] "Gestore mercati energetici: Results of the electricity market," <http://www.mercatoelettrico.org>, accessed on March 2019.
- [46] F. Adinolfi, F. D'Agostino, S. Massucco, M. Saviozzi, and F. Silvestro, "Advanced operational functionalities for a low voltage microgrid test site," in *IEEE Power & Energy Society General Meeting*, 2015.
- [47] F. Sossan, E. Namor, R. Cherkaoui, and M. Paolone, "Achieving the dispatchability of distribution feeders through prosumers data driven forecasting and model predictive control of electrochemical storage," *IEEE Trans. Sustain. Energy*, vol. 7, no. 4, pp. 1762–1777, Oct. 2016.